Advanced Normalization Tools for Cardiac Motion Correction

Nicholas J. Tustison, Yang Yang, and Michael Salerno

University of Virginia, Charlottesville VA 22903, USA

Abstract. We present our submission to the STACOM 2014 MoCo challenge for motion correction of dynamic contrast myocardial perfusion MRI. Our submission is based on the publicly available Advanced Normalization Tools (ANTs) specifically tailored for this problem domain. We provide a brief description with actual code calls to facilitate reproducibility. Time plots and K^{trans} values, based on the validation methodology of [11], are also provided to determine clinically relevant performance levels.

Keywords: ANTs, image registration, motion estimation, myocardial perfusion

1 Introduction

Motion correction for dynamic contrast MR myocardial perfusion is of significant research interest and has resulted in several techniques generally characterized as rigid or non-rigid image registration-based. To bring together interested researchers for discussion and comparison of methods for correction of motion artefacts and the development of performance benchmarks of such techniques, the STACOM 2014 workshop committee organized a motion correction challenge to be held in conjunction with MICCAI 2014.

We describe the submission of our non-rigid motion correction approach below which is both publicly available and open source.[1] This facilitates reproducibility for other researchers who wish to investigate the methods proposed and perhaps formulate configurations which improve existing performance levels.

2 Materials and Methods

2.1 Evaluation Data

As described by the challenge organizers:

> *The evaluation dataset consists of 10 cases from two centres: the University of Utah and University of Auckland. For each case, a single short axis slice time series at rest and at stress is provided. The Utah datasets*

[1] https://github.com/stnava/ANTs

were acquired using a saturation-recovery radial turboFLASH sequence at rest and during adenosine infusion (140 ?g/kg/min), as described in [5]. Contrast was 5 cc/s injection of Multihance (Gd-BOPTA) at 0.02 mmol/kg for the rest and 0.03 mmol/kg for the stress. Four of these subjects have known coronary artery disease. The Auckland cases were acquired using a saturation-recovery Cartesian turboFLASH sequence at rest and during adenosine infusion (140 µg/kg/min). Contrast was 0.04 mmol/kg Omniscan (gadodiamide). None of the Auckland cases have overt coronary disease. Expert-drawn contours only at a reference frame, chosen when contrast is present in both ventricles, were provided to the participants.

2.2 Preprocessing and Image Registration

We used the Advanced Normalization Tools (ANTs) package as the basis of our motion correction estimation framework as it provides a suite of utilities for image preprocessing and registration which have exhibited excellent performance in a variety of applications and challenges. For example, the popular Symmetric Normalization (SyN) algorithm [1, 2] performed well in a recent evaluation of popular deformable registration algorithms on human brain images [7]. Similarly, ANTs image registration and other capabilities were instrumental in recent MICCAI challenge performances including the lung-based EMPIRE10 (pulmonary CT) [9] and BRATS2013 (multimodal MRI, brain tumor) [8].

Normalization to the reference frame employs a pairwise registration strategy whereby each image is registered to its successive temporal neighbor using a recently developed SyN variation where the smoothing kernel is based on B-splines [14]. As originally formulated, the SyN transform is an explicit symmetrization of the well-known Large Deformation Diffeomorphic Metric Mapping (LDDMM) framework [4] which computes the geodesic solution between image pairs in the space of diffeomorphisms, i.e. differentiable mappings which have differentiable inverses [6]. One of the benefits of LDDMM (and SyN) is that it yields both the forward and inverse transforms between images I and J, which we denote as $I \underset{b}{\leftsquigarrow} J$ (where 'b' denotes "B-spline SyN"). Note that the image of the last time frame is registered to the image at the first time frame. Thus, to transform any image, I_t, at time point, t, to the reference image, I_R, temporally located at time, $t = r$, we simply concatenate the transforms either forwards

$$I_R \underset{b_r}{\leftsquigarrow} \underset{b_{r+1}}{\leftsquigarrow} \cdots \underset{b_{t-2}}{\leftsquigarrow} \underset{b_{t-1}}{\leftsquigarrow} I_t \tag{1}$$

or backwards

$$I_R \underset{b_{r-1}}{\leftsquigarrow} \underset{b_{r-2}}{\leftsquigarrow} \cdots \underset{b_{t+1}}{\leftsquigarrow} \underset{b_t}{\leftsquigarrow} I_t. \tag{2}$$

By concatenating transforms, only a single interpolation is performed for each normalization to the reference frame.

Given the temporal image variability and other confounds (e.g., noise), a multivariate image registration strategy was employed. Conventional image registration approaches are often limited to a single metric choice with a single "fixed" and "moving" image pair. In contrast, we use multiple image pairs and corresponding metrics which is made possible by recent developmental work to the Insight Toolkit [3]. These additional image pairs were created using several processing steps. Preprocessing for each image included N4 bias correction to minimize low frequency intensity variation artifacts commonly associated with MRI [15]. From each bias corrected image we created the following two images: (1) an image derived from a noise reduction filtering procedure meant to preserve structure [12] known as "SUSAN" from the FMRIB Software Library (FSL)[2] and (2) a Laplacian-based edge-detection image derived from the SUSAN image. A sample set of these images for one of the MoCo data is found in Figure 1.

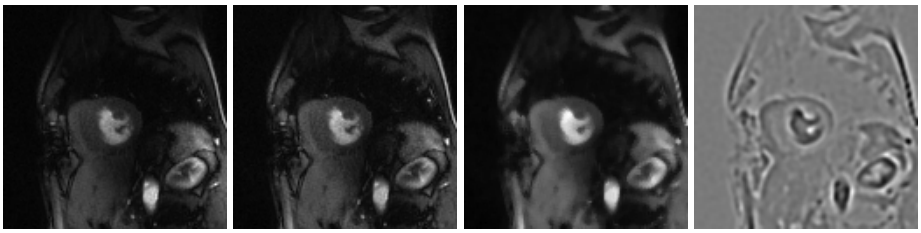

(a) (b) (c) (d)

Fig. 1. Sample auxiliary images from the MoCo data set (Subject 9 (Rest): Frame 23). Shown are the (a) original, (b) N4 bias corrected, (c) SUSAN, and (d) Laplacian images.

Each of these three sets of derived images are used to drive a deformable B-spline SyN pairwise registration for each temporal neighboring image pair where a weighted minimization of the three similarity metrics produced the resulting correspondence. For these data, we used equal weighting for each image pair/similarity metric which was based on a very limited heuristical assessment of the data. Investigation into relative weighting schemes might increase performance levels particularly for varying data qualities. For example, given less noisy data, decreasing the weighting of the contribution of the SUSAN-based image pairing might be helpful as noise would be less of a factor.

This process is most clearly described by the `antsRegistration` program call given in Listing 1.1.[3] Each fixed and moving image pair was histogram matched

[2] http://fsl.fmrib.ox.ac.uk/fsl/fslwiki/

[3] In many situations, the deformable registration portion of the total alignment strategy is preceded by one or more linear registrations (e.g., center of mass alignment, affine registration). This is easily accommodated into the `antsRegistration` command line syntax. However, for this specific problem domain, it was found that such pre-deformable alignment steps were unnecessary.

[10] and intensity-truncated to b extreme values. The choice of similarity metric for each image pair was motivated by the characteristics of each individual set and the need to balance an aggressive alignment of strong image features while minimizing displacements caused by incorrect correspondences. The N4 bias corrected images were incorporated into the motion correction strategy since they were closest to the original imaging data. Given the relative amount of noise, we used a neighborhood cross correlation (CC) metric (window radius = 6 voxels) which evaluates the linear intensity relationship between neighborhood regions at corresponding points in the image pair. This metric is the default similarity metric choice used in ANTs-based image registration [1] and helps mitigate the effects of noise. In contrast, because of the smoothing effects of SUSAN and the Laplacian filtering, we used the more aggressive Demons metric [13] which can be viewed as a second order minimization of the sum-of-squared differences (SSD) objective function.

A multi-resolution approach consisting of three levels with each successive level corresponding to double the resolution of the previous level was used with varying isotropic smoothing used at each level. For specific parameter choices, we refer the reader to Listing 1.1.

```
// Input image pairs include:
//  * N4 bias corrected
//  * Structure-preserving noise reduction (SUSAN) of N4 images
//  * Laplacian filtering of N4 images.

antsRegistration --dimensionality 2
                 --output ${registrationPrefix} \
                 --winsorize-image-intensities [0.01,0.99] \
                 --use-histogram-matching 1 \
                 --transform BSplineSyN[0.1,2x2,0] \
                 --metric CC[${n4Fixed},${n4Moving},1,6] \
                 --metric Demons[${susanFixed},${susanMoving},1,1] \
                 --metric Demons[${laplacianFixed},${laplacianMoving},1,1] \
                 --convergence [100x70x50,1e-8,10] \
                 --shrink-factors 4x2x1 \
                 --smoothing-sigmas 1x0.5x0vox
```

Listing 1.1. `antsRegistration` call used for the pairwise registration.

Once all the pairwise transforms are generated between each set of temporal neighbors, we normalize all the original images to the reference frame by concatenating all the transforms using the program `antsApplyTransforms` which performs only a single interpolation per normalization regardless of the number of transforms specified.

3 Evaluation

As described by the challenge organizers:

> *We will validate the motion correction algorithms based on flow indices. That is, the registered datasets will be processed to*
> - *create time curves for each of 6 tissue regions,*
> - *create an arterial input function (AIF) from the automatically determined blood pool curves within the endocardial border,*

– *subtract off the average of the initial pre-contrast frames and normalize by estimated coil sensitivity differences so that the time curves are proportional to gadolinium concentration, and*
– *fit the data to a compartment model to obtain myocardial blood flow MBF in ml/g/min [11].*

The score will be the sum of squared differences of the Myocardial Blood Flow (MBF) index with the registration method, compared to MBF of a pseudo-gold standard obtained from manually drawn contours from experienced analysts.[4]

Implementation of the validation methodology was provided by the workshop organizers which were applied to all motion-corrected 10 gated image sets and the single ungated data set. The resulting time curves and model fits are given in Figures 2, 3, and 4 with the K^{trans} values given in Tables 1.

Table 1. K^{trans} values for all data for all 6 ROIs.

	ROI_1	ROI_2	ROI_3	ROI_4	ROI_5	ROI_6
MoCo_01 (rest)	0.7646	0.793	0.6472	0.6223	1.1396	0.6169
MoCo_01 (stress)	2.991	3.3591	3.3946	3.8864	3.6427	2.9233
MoCo_02 (rest)	1.26	0.8393	0.8038	0.8026	0.621	0.9659
MoCo_02 (stress)	3.6184	4.7307	2.4689	2.1684	2.0884	4.6189
MoCo_03 (rest)	1.3238	1.0138	1.9537	1.4278	0.6698	1.2323
MoCo_03 (stress)	4.6317	4.482	2.5719	2.2236	1.2169	3.3639
MoCo_04 (rest)	2.4826	1.958	1.7667	2.0848	3.0735	2.516
MoCo_04 (stress)	6.6083	10.1963	9.2774	10.0296	10.7357	8.875
MoCo_05 (rest)	1.6678	1.4952	0.8095	0.8683	1.1663	1.318
MoCo_05 (stress)	2.4283	2.6987	2.0908	1.9775	2.3872	3.0467
MoCo_06 (rest)	0.9946	1.2878	1.1367	0.7262	0.8156	0.865
MoCo_06 (stress)	2.1543	2.6292	2.1322	2.59	1.4002	1.4648
MoCo_07 (rest)	0.6009	0.5397	0.4214	0.2904	0.8107	1.234
MoCo_07 (stress)	2.8381	2.2815	1.8141	1.7029	2.7065	2.8503
MoCo_08 (rest)	1.0315	0.8754	0.7959	0.7106	0.9726	1.0769
MoCo_08 (stress)	3.1103	2.9066	2.2222	2.369	2.4781	1.796
MoCo_09 (rest)	1.0073	0.8589	0.7194	0.8689	1.1375	1.1258
MoCo_09 (stress)	1.939	0.9883	1.0515	1.6527	1.9416	2.2943
MoCo_10 (rest)	2.734	2.3579	2.2832	2.3316	2.822	2.743
MoCo_10 (stress)	2.2161	3.8051	2.9618	2.234	5.6507	2.9052
Ungated	2.3471	3.0672	2.6664	3.7773	3.5338	2.7093

[4] http://www.cardiacatlas.org/web/stacom2014/moco-validation

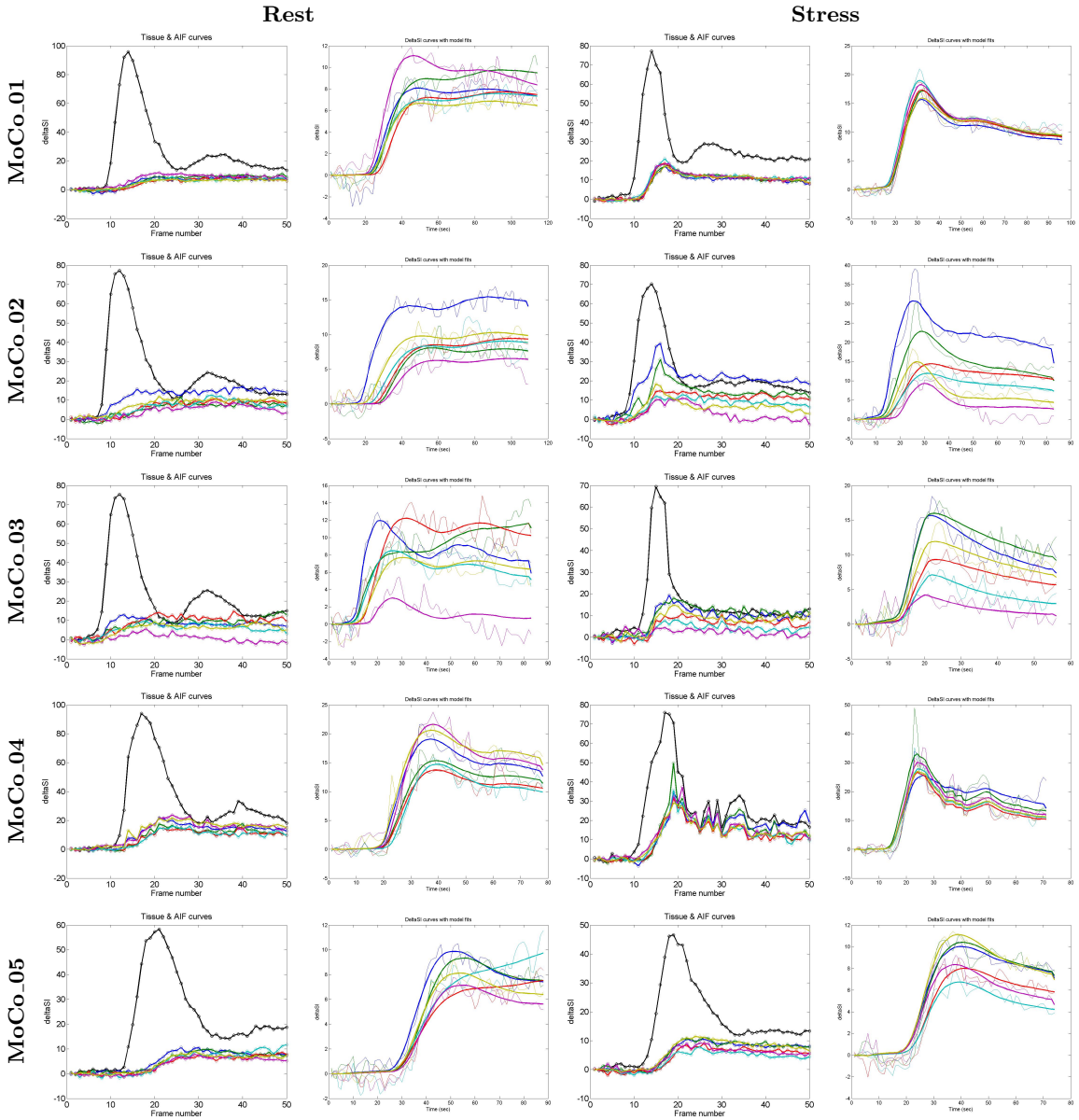

Fig. 2. Validation time curves consisting of tissue and arterial input function time plots for the first five gated data sets.

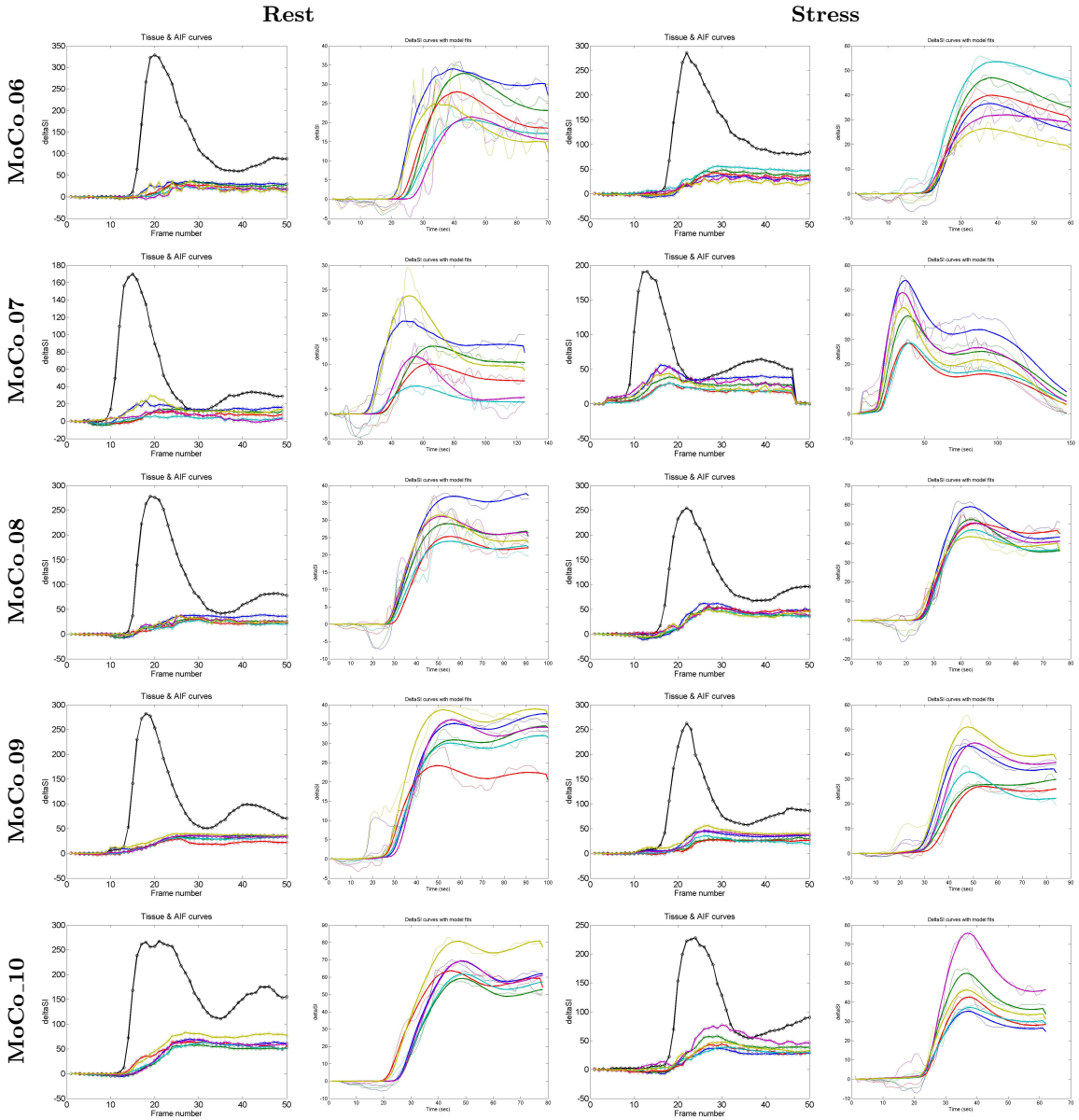

Fig. 3. Validation time curves consisting of tissue and arterial input function time plots for the gated data sets 6–10.

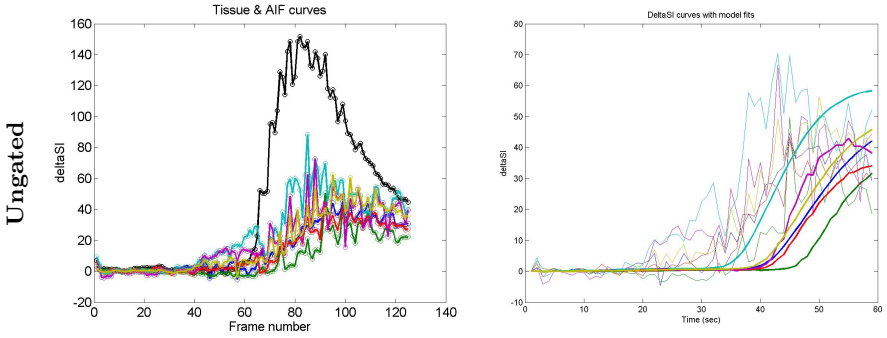

Fig. 4. Validation time curves consisting of tissue and arterial input function time plots for the ungated data set.

4 Discussion and Conclusions

Based on visual assessment, our correction motion method seems to work well. However, such qualitative verification is far from ideal as the true measure of its utility is tied directly to its ability to produce useful clinical measures (hence, the motivation for the validation framework provided by the organizers). Comparison of our results with results produced by other teams will certainly prove useful in assessing the proposed methods.

Confounds such as noise, through-plane motion, and lack of contrast caused errors during the alignment optimization over all subjects. For example, in the ungated case shown in Figure 5 there is definite motion between frames $t = 77$ and $t = 78$ (wall thinning) which is not captured by our methodology. This is

$t = 77$ $t = 78$ $t = 85$

Fig. 5. Wall thinning between $t = 77$ and $t = 78$ not captured by the proposed ANTs registration configuration. For completeness, we show the reference image ($t = 85$).

to be expected given the conservative approach to minimize the effects of noise. However, considering the different motion characteristics between the two types

of data, the heuristically-chosen optimal parameters selected for the gated data might be suboptimal for the ungated data. Further investigation with additional ungated data would be necessary for tuning a different, targeted set of parameters.

One other major potential issue with our method is the dependency on good pairwise normalizations to be able to infer correct correspondences back to the reference frame. Any error in the chain of transforms will be propagated in normalizing a particular image back to the reference frame. The general principle of incorporating prior knowledge to improve solution strategies is definitely an avenue we are pursuing for future work. One extension we are currently investigating is the use of optimal shape and intensity templates derived from the subject image data. By coalescing similar images into subgroups of optimal templates and calculating the transforms between them, optimal transformation paths between images can be found using graph-theoretic methods.

References

1. Avants, B.B., Epstein, C.L., Grossman, M., Gee, J.C.: Symmetric diffeomorphic image registration with cross-correlation: evaluating automated labeling of elderly and neurodegenerative brain. Med Image Anal 12(1), 26–41 (Feb 2008)
2. Avants, B.B., Tustison, N.J., Song, G., Cook, P.A., Klein, A., Gee, J.C.: A reproducible evaluation of ANTs similarity metric performance in brain image registration. Neuroimage 54(3), 2033–44 (Feb 2011)
3. Avants, B.B., Tustison, N.J., Stauffer, M., Song, G., Wu, B., Gee, J.C.: The Insight ToolKit image registration framework. Front Neuroinform 8, 44 (2014)
4. Beg, M.F., Miller, M.I., Trouve, A., Younes, L.: Computing large deformation metric mappings via geodesic flows of diffeomorphisms. International Journal of Computer Vision 61(2), 139–157 (2005)
5. DiBella, E.V.R., Fluckiger, J.U., Chen, L., Kim, T.H., Pack, N.A., Matthews, B., Adluru, G., Priester, T., Kuppahally, S., Jiji, R., McGann, C., Litwin, S.E.: The effect of obesity on regadenoson-induced myocardial hyperemia: a quantitative magnetic resonance imaging study. Int J Cardiovasc Imaging 28(6), 1435–44 (Aug 2012)
6. Dupuis, P., Grenander, U.: Variational problems on flows of diffeomorphisms for image matching. Q. Appl. Math. LVI, 587–600 (1998)
7. Klein, A., Andersson, J., Ardekani, B.A., Ashburner, J., Avants, B., Chiang, M.C., Christensen, G.E., Collins, D.L., Gee, J., Hellier, P., Song, J.H., Jenkinson, M., Lepage, C., Rueckert, D., Thompson, P., Vercauteren, T., Woods, R.P., Mann, J.J., Parsey, R.V.: Evaluation of 14 nonlinear deformation algorithms applied to human brain MRI registration. Neuroimage 46(3), 786–802 (Jul 2009)
8. Menze, B., Jakab, A., Bauer, S., Kalpathy-Cramer, J., Farahani, K., Kirby, J., Burren, Y., Porz, N., Slotboom, J., Wiest, R., Lanczi, L., Gerstner, E., Weber, M.A., Arbel, T., Avants, B., Ayache, N., Buendia, P., Collins, L., Cordier, N., Corso, J., Criminisi, A., Das, T., Delingette, H., Demiralp, C., Durst, C., Dojat, M., Doyle, S., Festa, J., Forbes, F., Geremia, E., Glocker, B., Golland, P., Guo, X., Hamamci, A., Iftekharuddin, K., Jena, R., John, N., Konukoglu, E., Lashkari, D., Antonio Mariz, J., Meier, R., Pereira, S., Precup, D., Price, S., Riklin-Raviv, T., Reza, S., Ryan, M., Schwartz, L., Shin, H.C., Shotton, J., Silva, C., Sousa,

N., Subbanna, N., Szekely, G., Taylor, T., Thomas, O., Tustison, N., Unal, G., Vasseur, F., Wintermark, M., Hye Ye, D., Zhao, L., Zhao, B., Zikic, D., Prastawa, M., Reyes, M., Van Leemput, K.: The multimodal brain tumor image segmentation benchmark (BRATS) (2014), http://hal.inria.fr/hal-00935640

9. Murphy, K., van Ginneken, B., Reinhardt, J.M., Kabus, S., Ding, K., Deng, X., Cao, K., Du, K., Christensen, G.E., Garcia, V., Vercauteren, T., Ayache, N., Commowick, O., Malandain, G., Glocker, B., Paragios, N., Navab, N., Gorbunova, V., Sporring, J., de Bruijne, M., Han, X., Heinrich, M.P., Schnabel, J.A., Jenkinson, M., Lorenz, C., Modat, M., McClelland, J.R., Ourselin, S., Muenzing, S.E.A., Viergever, M.A., De Nigris, D., Collins, D.L., Arbel, T., Peroni, M., Li, R., Sharp, G.C., Schmidt-Richberg, A., Ehrhardt, J., Werner, R., Smeets, D., Loeckx, D., Song, G., Tustison, N., Avants, B., Gee, J.C., Staring, M., Klein, S., Stoel, B.C., Urschler, M., Werlberger, M., Vandemeulebroucke, J., Rit, S., Sarrut, D., Pluim, J.P.W.: Evaluation of registration methods on thoracic CT: the EMPIRE10 challenge. IEEE Trans Med Imaging 30(11), 1901–20 (Nov 2011)
10. Nyúl, L.G., Udupa, J.K., Zhang, X.: New variants of a method of MRI scale standardization. IEEE Trans Med Imaging 19(2), 143–50 (Feb 2000)
11. Pack, N.A., DiBella, E.V.R.: Comparison of myocardial perfusion estimates from dynamic contrast-enhanced magnetic resonance imaging with four quantitative analysis methods. Magn Reson Med 64(1), 125–37 (Jul 2010)
12. Smith, S.M., Brady, J.M.: SUSAN - a new approach to low level image processing. International Journal of Computer Vision 23(1), 45–78 (May 1997)
13. Thirion, J.P.: Image matching as a diffusion process: an analogy with Maxwell's demons. Med Image Anal 2(3), 243–60 (Sep 1998)
14. Tustison, N.J., Avants, B.B.: Explicit B-spline regularization in diffeomorphic image registration. Front Neuroinform 7, 39 (2013)
15. Tustison, N.J., Avants, B.B., Cook, P.A., Zheng, Y., Egan, A., Yushkevich, P.A., Gee, J.C.: N4ITK: improved N3 bias correction. IEEE Trans Med Imaging 29(6), 1310–20 (Jun 2010)